

Sodiophilic amyloid fibril modified separator for dendrite-free sodium metal batteries

*Jinming Wang, Yan Gao, Di Liu, Guodong Zou, Lanjie Li, Carlos Fernandez, Qingrui Zhang, Raffaele Mezzenga, Qiuming Peng**

J.M. Wang, Y. Gao, D. Liu, G.D. Zou, Q.R. Zhang, Q.M. Peng

State Key Laboratory of Metastable Materials Science and Technology, Yanshan University,
Qinhuangdao, 066004, P.R. China

Corresponding Authors: pengqiuming@ysu.edu.cn

L.J. Li

Chengde Iron and Steel Group Co., Ltd, HBIS Group Co., LTD., Chengde, Hebei 067102,
China

C. Fernandez

School of Pharmacy and Life Sciences, Robert Gordon University, Aberdeen, AB107GJ,
United Kingdom

R. Mezzenga

Laboratory of Food and Soft Materials, Department of Health Sciences and Technology, ETH
Zurich, Schmelzbergstrasse 9, Zurich 8092, Switzerland

Materials and Methods

Synthesis of Amyloid Fibrils

β -lactoglobulin was purified from whey protein isolate received as a kind donation from Fonterra, New Zealand. To remove non-"native" proteins, the following procedure was performed. Initially, the protein powder was dissolved in deionized water at a concentration of 10 wt.%. Subsequently, the solution was adjusted to pH 4.6 utilizing a 1 M HCl solution, and stirred at 40 °C for a duration of 4 hours. The supernatant was then collected through high-speed centrifugation (8000 rpm, 20 min) using a centrifuge. Finally, the pH of the supernatant was adjusted to 2 with a 1 M HCl solution.

To eliminate possible residual insoluble protein, the supernatant was filtered through a 0.45 μ m Millipore filter. Dialysis was then conducted utilizing a membrane (spectra/por dialysis MWCO: 6–8 kDa) to remove the ionic species until the solution pH reached a value range of 4.5–4.8. Afterward, the pH was readjusted to 2, and the solution was freeze-dried to acquire protein monomers. Finally, the desired amyloid fibrils were obtained by heating protein monomers at 90 °C for 1, 5, and 10 hours (AF1, AF5, AF10).

Synthesis of Amyloid Fibrils@Glass Fiber Separator

Commercial glass fiber (GF) separator was purchased from GE-Whatman Company (UK. GF/D, nominal rating, 2.7 μ m; Herzberg, 41 s; Gurley value, 2.2 s/100 min; thickness, 675 μ m; weight, 121 g m⁻²). Subsequently, amyloid fibrils solution (1 wt.%, 2 wt.%, 5 wt.%; 2 ml) was dropped onto the GF separator using the vacuum filtration method, yielding the amyloid fibrils@GF separator (AF@GF). Specifically, the deposition process of AFs on the separator was conducted through vacuum filtration, utilizing a filtration bottle connected to a circulating water vacuum pump (Figure S1). Initially, the protein solution was cautiously added dropwise onto the GF separator, and the AFs were bound to the GF separator by means of the vacuum filtration device. The aqueous solvent passed through the GF separator and trickled into the filtration bottle underneath, effectively eliminating most of the water from the

protein solution. Subsequently, the resulting composite separator was frozen and freeze-dried at $-80\text{ }^{\circ}\text{C}$ for 2 days to obtain the final AFs@GF separator.

Materials Characterizations

FT-IR spectrometer (Nexus 870, USA) was used to detect the types of functional groups on the amyloid fibrils powder with an adsorption wavelength range of $1000\text{-}4000\text{ cm}^{-1}$. XPS measurements of amyloid fibrils were carried out on an X-ray photoelectron spectrometer (XPS, Thermo Scientific Escalab 250Xi) using monochromatic Al $K\alpha$ X-Ray source. The binding energies obtained in the XPS analysis were corrected by referencing the C 1s peak position (284.48 eV). Raman spectroscopy was obtained from micro-Raman spectroscopy (Horiba, HR Evolution) with a laser radiation of 514 nm . X-ray diffraction patterns were recorded with the X-ray diffractometer equipment (Rigaku D/MAX-2005/PC) using Cu $K\alpha$ radiation ($\lambda = 1.5406\text{ \AA}$) with a step scan of 0.02° per step and a scan rate of $4^{\circ}\text{ min}^{-1}$. Microstructure morphology and element analysis were observed by scanning electron microscopy (FEI Helios G4CX) with an accelerating voltage of 5 kV for SEM image capture and 20 kV for EDX mapping. Transmission electron microscopy (TEM) analysis was performed on a FEI Talos F200 operated at 200 kV . Tensile tests were conducted using a tensile stage controller (Shenzhen Sansi UTM4103) with a 20 N load cell at a crosshead speed of 0.5 mm min^{-1} . The elastic moduli of the separators were quantified using peak force quantitative nanomechanics (PFQNM) mode on an AFM (Bruker Dimension Icon with ScanAsyst), and subsequently analyzed using Nanoscope Analysis software. PeakForce tapping mode was adopted in AFM imaging using a ScanAsyst-Air silicon probe. Force spectroscopy mode was utilized to obtain force curves of the samples, with a typical scanning rate of 0.5 Hz and a loading force of 0.5 nN . To ensure accuracy, data was collected at various positions on at least three separate samples, and the moduli of the separators were estimated based on the collected data.

In-situ XRD characterization in Na|Al half batteries assembled with the AF5@GF separator or the GF separator: The *in-situ* XRD measurements were obtained at X-ray diffractometer equipment (D8 ADVANCE, Bruker AXS GmbH Co., Ltd). The Na|Al half battery was assembled using a tailor-made mold with a window for X-ray penetration. The constant galvanostatic discharge curve of the Na|Al half battery was measured by electrochemical workstation (Bio-logic, VSP), and the current density was 1 mA cm^{-2} . The XRD patterns recording frequency was 10 min for the same position.

Electrochemical Measurements

The electrochemical performance was tested by assembling the CR2032 coin-type full cell. The thickness of Na foils in the experiment is $100 \text{ }\mu\text{m}$ (capacity is 11.3 mAh cm^{-2} ; capacity = foil thickness \times ρ_{Na} \times theoretical capacity = $100 \times 10^{-4} \text{ cm} \times 0.97 \text{ g cm}^{-3} \times 1165 \text{ mAh g}^{-1} = 11.3 \text{ mAh cm}^{-2}$). All electrochemical data including cycling tests of Na|Na symmetric batteries, Na|Al half batteries and full cells were measured on a Land CT2001A battery test system at room temperature. For batteries testing, the ester-based electrolyte which consists of 1.0 M NaClO_4 in EC:DEC=1:1 vol.% with 5.0 wt. % FEC was employed. For the full-cell cathode, the slurry of cathode materials was prepared by mixing 80 wt. % $\text{Na}_3\text{V}_2(\text{PO}_4)_3$ (NVP) as the active material, 10 wt. % Super P, and 10 wt. % polyvinylidene difluoride (PVDF) as the binder in N-methylpyrrolidone (NMP). Then, the slurry was coated on an aluminum foils substance, followed by drying at $80 \text{ }^\circ\text{C}$ for 12 h in a vacuum oven. The mass loading of active materials in cathodes was controlled to 5 mg cm^{-2} . Moreover, the capacities are calculated based on the mass of NVP in cathode. The working potential window of the full cell was from 2.5 to 3.8 V. In addition, the *ex-situ* electrochemical impedance spectroscopy (EIS) measurements of Na|Na symmetric batteries were carried out via Biologic VMP3 system between 100 kHz and 0.01 Hz. The ionic conductivity of interfacial protective layers was measured using the same method, and the equation used was $\sigma = d/R \times S$, where d is the thickness of the measured sample (cm); R is the intrinsic impedance of the measured

sample (ohm), and S is the effective area of the electrode (cm^2). To determine the Na^+ transference number (t_{Na^+}), we employed chronoamperometry with a $\text{Na}||\text{Na}$ symmetric cell, which was subjected to a constant step potential (ΔV) of 10 mV. The transference number was then calculated using the following equation, which is consistent with the approach outlined by Bruce and Vincent:

$$t_{\text{Na}^+} = I_S(\Delta V - I_0 R_0) / I_0(\Delta V - I_S R_S)$$

Where, I_0 and I_S is the initial-and steady-state current, respectively, ΔV is the applied constant potential (10 mV), R_0 and R_S is the initial- and steady-state interfacial impedance of the cell determined by EIS tests, respectively. *In-situ* EIS measurements of full cells were performed using an electrochemical workstation (Biologic VMP3) with an amplitude of 50 mV, and data were recorded every 8 minutes. The frequency range of the measurements was 100 kHz to 0.01 Hz. In addition, charge and discharge EIS tests were conducted in galvanostatic mode with a current density of 1C (117.6 mAh g^{-1}).

COMSOL Simulation

Finite element simulations were performed using the tertiary current distribution module of COMSOL Multiphysics software. Ion transport was calculated by the Nernst-Planck equation, and the Butler-Volmer equation was used to solve the surface reaction kinetics. According to Faraday's law, the flux at the electrolyte boundary was coupled to the electrochemical reaction. The electric field driven Na^+ migration was described by the Nernst-Planck equation. The simulation area near the Al electrode is set to $19 \times 18 \mu\text{m}$. The current density coming from electrolyte is set to 0.5 mA cm^{-2} . The Na^+ concentration of the electrolyte is set to 1M. The diffusion coefficients of Na^+ in the electrolyte and the amyloid fibril are $8 \times 10^{-15} \text{ m}^2 \text{ s}^{-1}$ and $1.65 \times 10^{-8} \text{ m}^2 \text{ s}^{-1}$, respectively. The conductivity of the electrolyte and the amyloid fibril are set to $4.52 \times 10^{-3} \text{ S m}^{-1}$ and $3.06 \times 10^{-3} \text{ S m}^{-1}$, respectively. The model is solved in the solver COMSOL Multiphysics. The governing equations are as follows:

$$\nabla \cdot (-D_i \nabla c_i - z_i u_{m,i} F c_i \nabla V) + u \cdot \nabla c_i = R_i$$

$$\nabla \cdot N^V = F \sum_i z_i R_i$$

$$\sum_i z_i c_i = 0$$

$$N^V = F \sum_i z_i (-D_i \nabla c_i - z_i u_{m,i} F c_i \nabla V)$$

where, N_i is the mass flux for each species, D_i is the diffusion coefficient, c_i is the concentration, z_i is the charge number, V is the electrolyte potential, F is Faraday constant. Convection is not considered in this process, so u is 0. The model is solved in the solver COMSOL multiphasic.

Computational Method

The DFT calculations were performed by VASP based on projector augmented wave (PAW) methodology. The PBE exchange-related generalized functions within the generalized gradient approximation (GGA) are used. The cutoff energy for the kinetic energy was 500eV. By the Monkhorst-Pack method, the k-mesh in the Brillouin zone is 5 x 5 x 1. The energy convergence tolerance was 1.0×10^{-5} eV/atom, and the force certification was 0.01 eV/Å. CIF values of 2108012, 2311101, and 2004822 for leucine, alanine and glutamine respectively.

The binding energy (ΔE_b) was calculated as following:

$$\Delta E_b = E_{\text{adsorbate+support}} - (E_{\text{support}} + E_{\text{adsorbate}})$$

where $E_{\text{adsorbate+support}}$ was the total energy of the materials with adsorbed molecule, E_{support} and $E_{\text{adsorbate}}$ were the energy of the leucine/alanine/glutamine and chemical potential of Na.



Figure S1. Vacuum filtration device used when AFs are deposited on the separator.

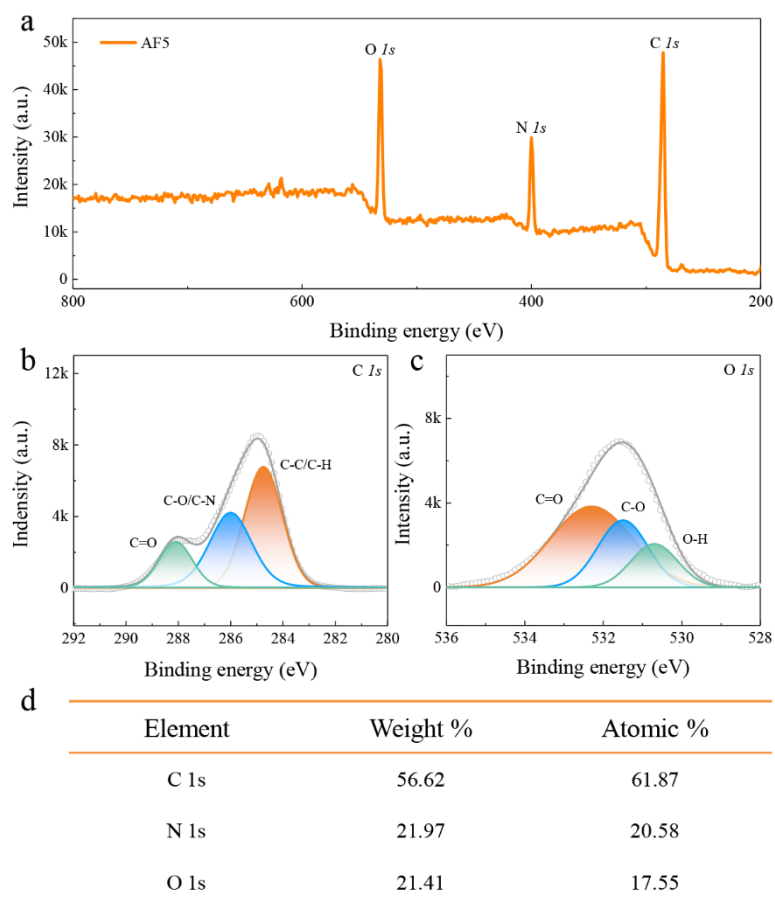


Figure S2. (a) XPS full spectrum of AF5. (b-c) XPS spectrum of AF5 of *C 1s* (b) and *O 1s* (c). (d) Contents of various elements in AF5 by XPS semi-quantitative analysis.

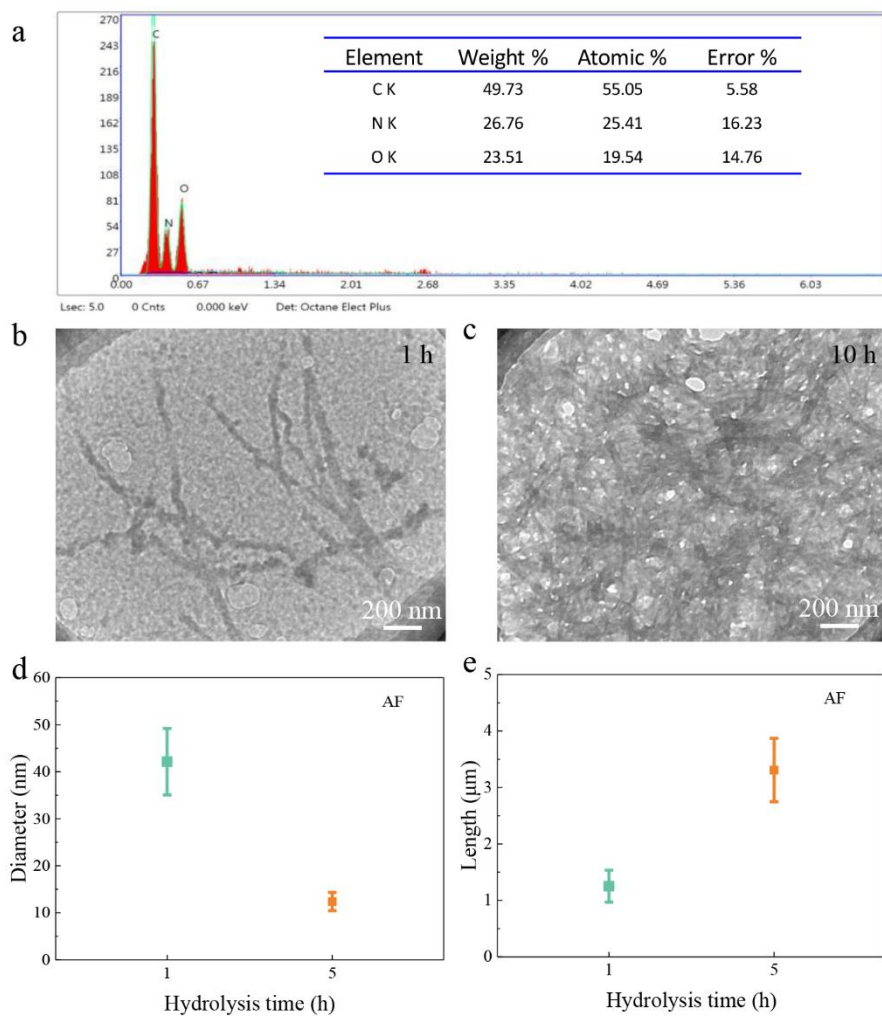


Figure S3. (a) Contents of various elements in AF5 analyzed by EDS. (b-c) TEM images of amyloid fibrils hydrolyzed for 1 hour (b) and 10 hours (c). (d-e) Diameter (d) and length (e) of amyloid fibrils hydrolyzed for 1 hour and 5 hours.

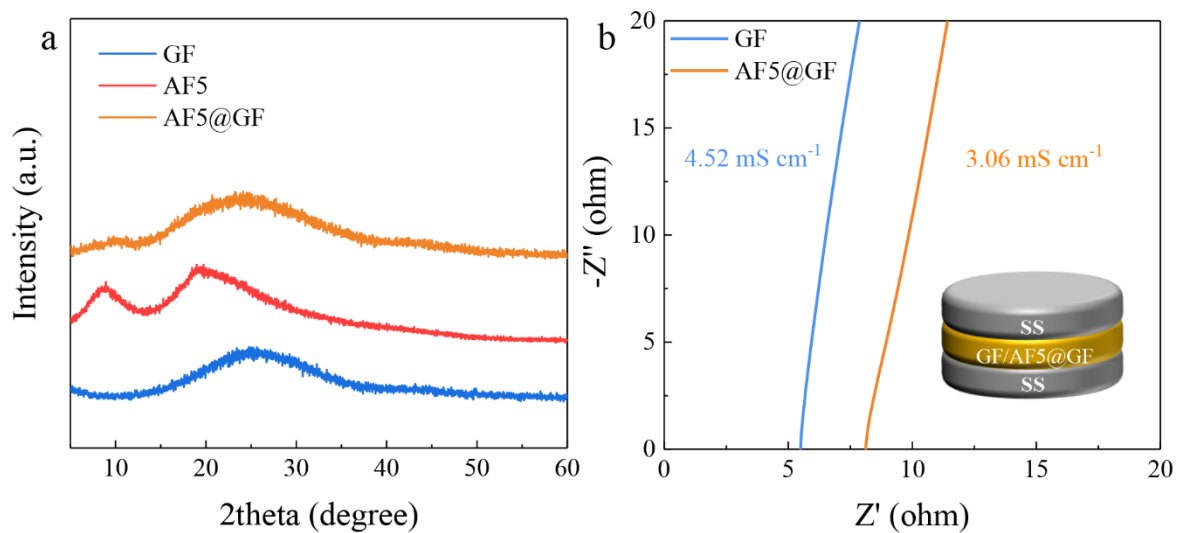


Figure S4. (a) XRD patterns of AF5, AF5@GF, and GF. (b) Ionic conductivity of AF5@GF, and GF measured through impedance spectroscopy by assembling a cell of stainless steel/separators/stainless steel. (c-d) SEM morphology of the cross-section of AF@GF (c) and GF (d).

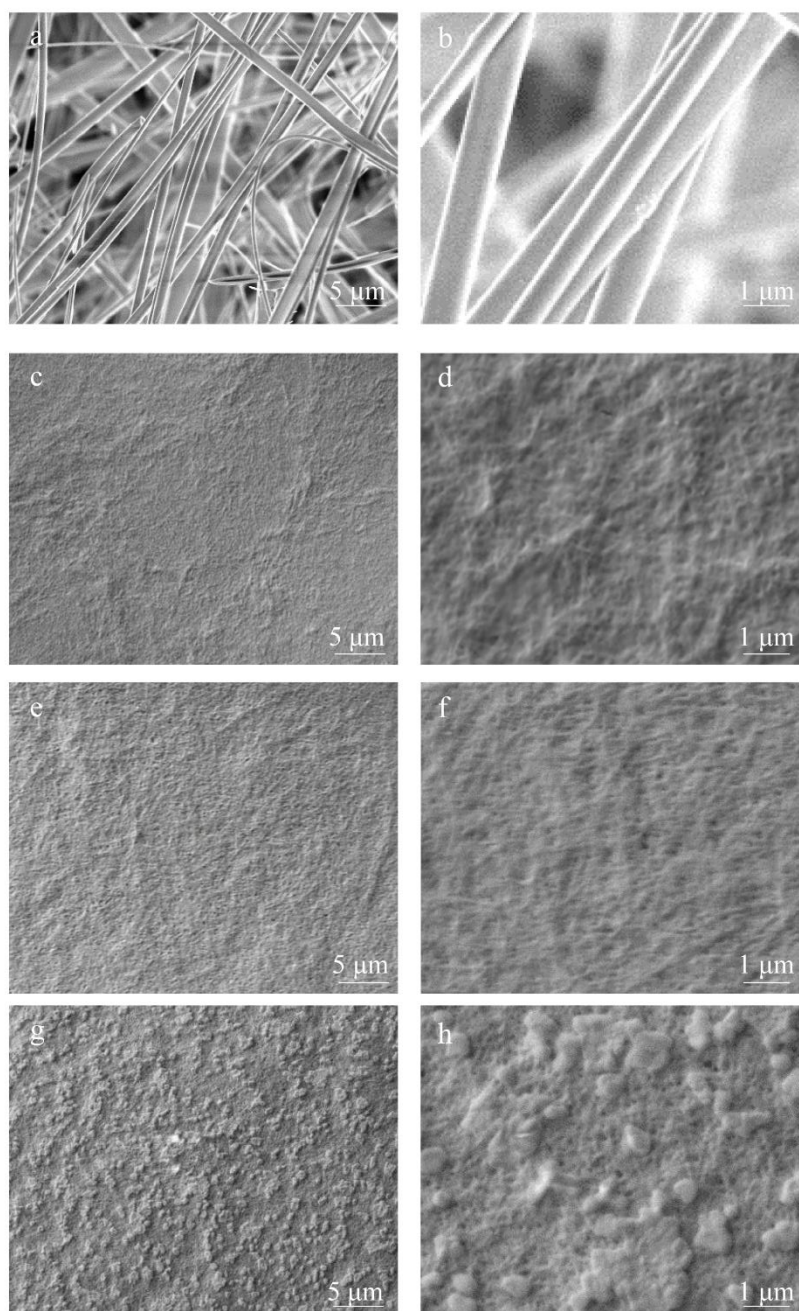


Figure S5. SEM morphology of the surface of GF (a, b), AF5@GF-1 wt. % (c, d), AF5@GF-2 wt. % (e, f), and AF5@GF-5 wt. % (g, h).

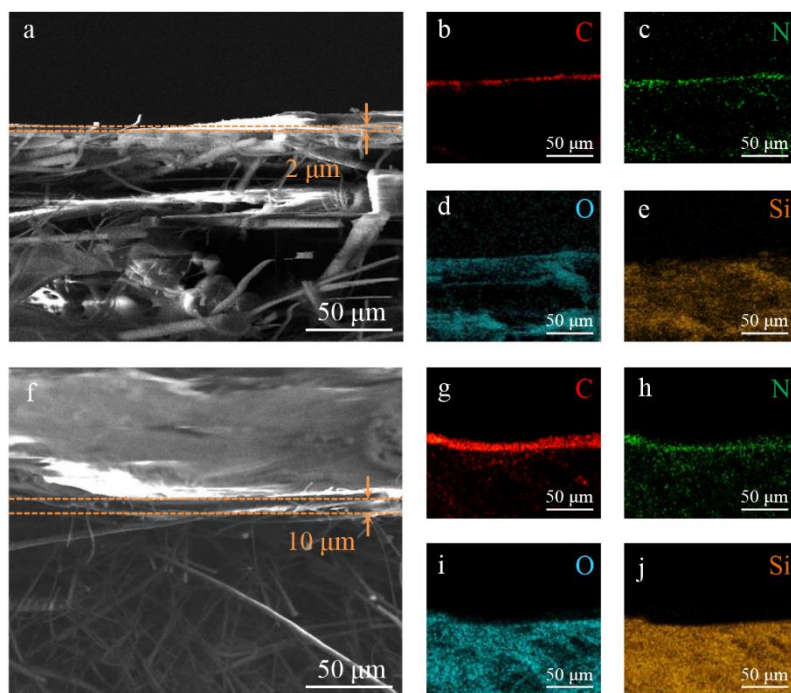


Figure S6. Longitudinal-section SEM image and corresponding mapping of the AF5@GF separator-1 wt. % (a-e), AF5@GF separator-5 wt. % (f-j).

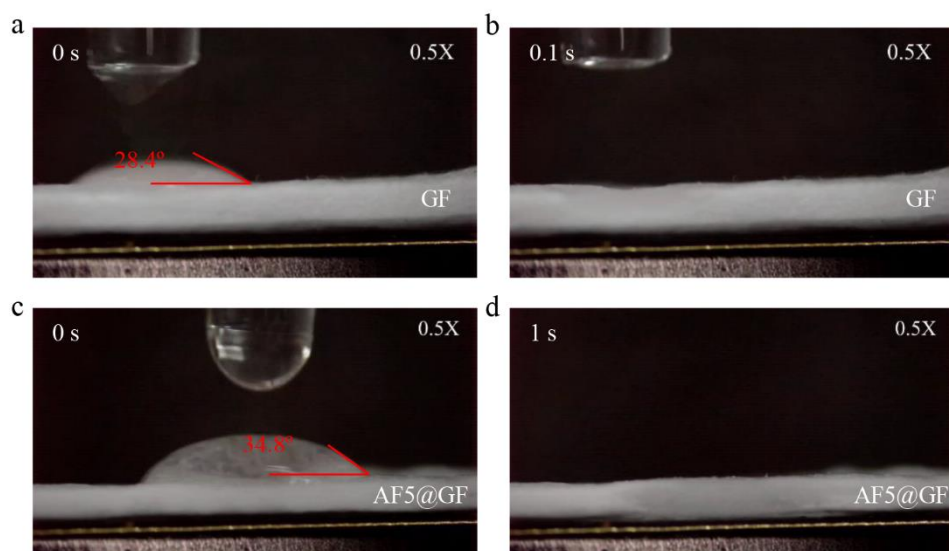


Figure S7. Contact angles of the electrolyte on GF and AF5@GF separators.

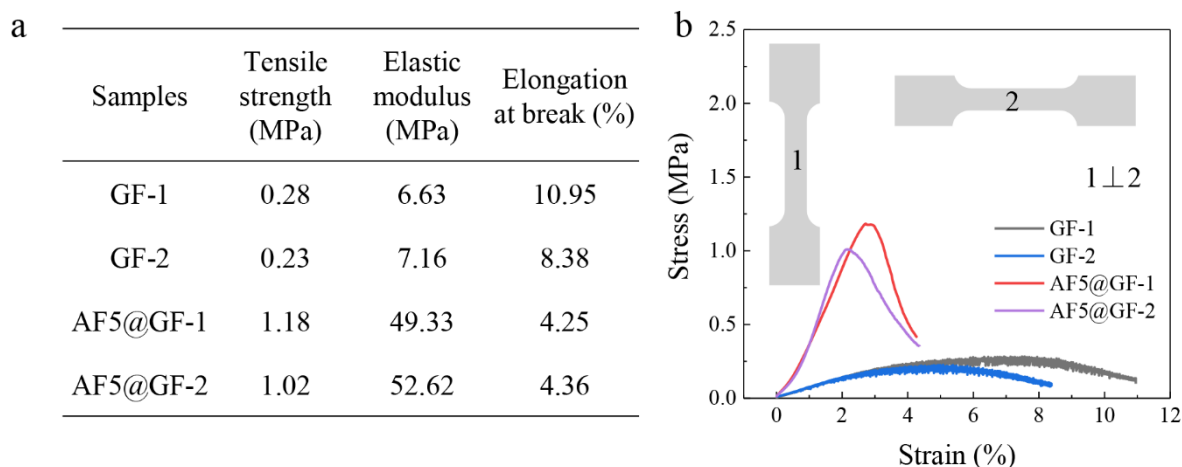


Figure S8. (a) Summary table of tensile mechanical properties of AF@GF and GF separators. (b) Stress-strain curves of AF@GF and GF separators. Inset: Schematic diagrams of the tensile specimen shapes of samples 1 and 2, and their corresponding crop orientations.

Note: the cropping directions of the AF5@GF separators in these two tests were perpendicular to each other (Samples 1 \perp Samples 2). The experimental results indicate that there is minimal difference between the two test results: the tensile strength is 1.18MPa and 1.02MPa, the modulus of elasticity is 49.33MPa and 52.62MPa, and the elongation at break is 4.25% and 4.36%, respectively. This suggests that the orientation of the amyloid fibrils complexed on the GF separator is disordered.

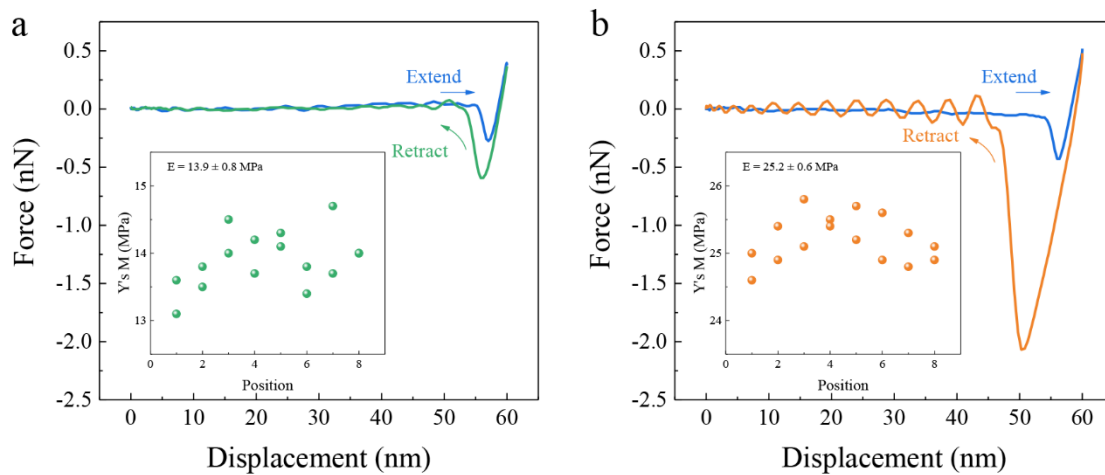


Figure S9. Typical force-displacement curves of GF (a) and AF5@GF (b) separators.

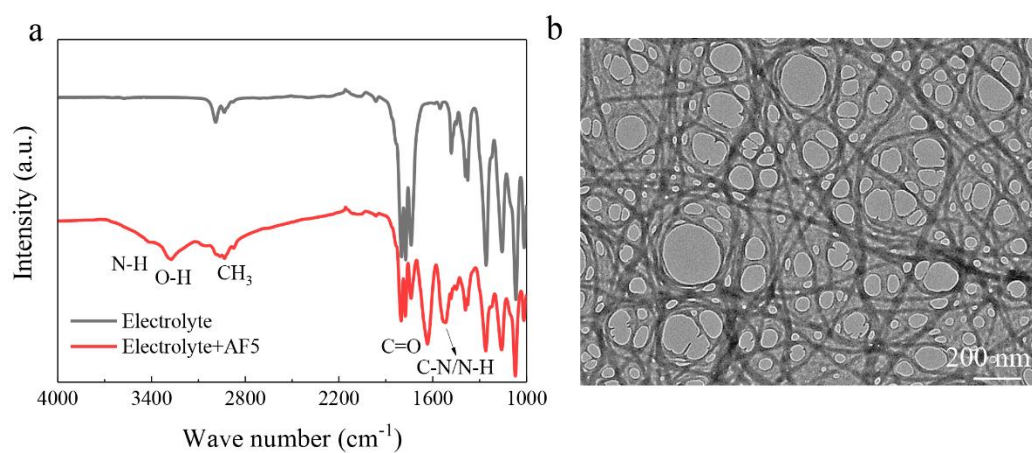


Figure S10. (a) FTIR spectrum of AF5 after immersion in electrolyte for 24 hours. (b) TEM morphology of AF5 after immersion in electrolyte for 24 hours.

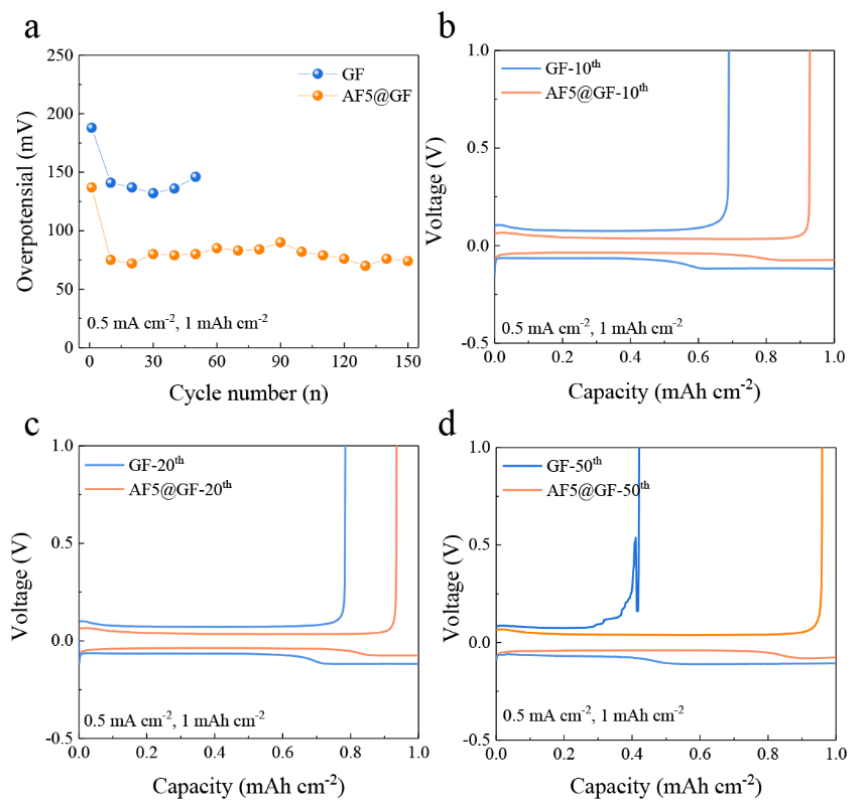


Figure S11. (a) Comparison of the stripping/deposition overpotentials of Na|Al half cells equipped with AF5@GF separator and GF separator. (b-d) Voltage profiles of Na stripping/plating of Al collector equipped with AF5@GF separator or GF separator at the (b) 10th, (c) 20th and (d) 50th.

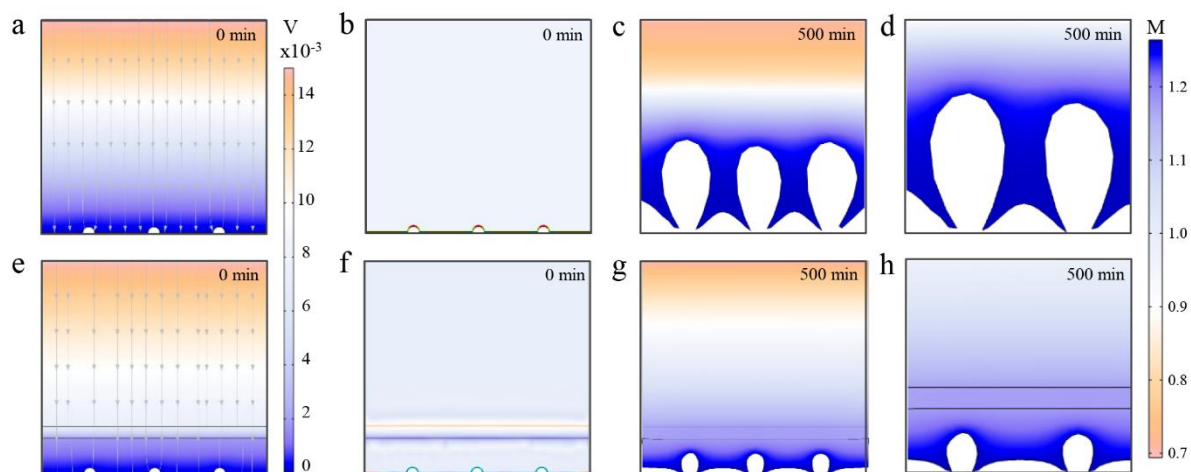


Figure S12. (a, e) Simulate the electric field distribution on Na anode without AF5 (a) and with AF5 (e) after 0 min. Simulate the Na ion distribution on Na anode without AF5 (b-d) and with AF5 (f-h) after 0 min (b, f) or after 500 min (c-d, g-h).

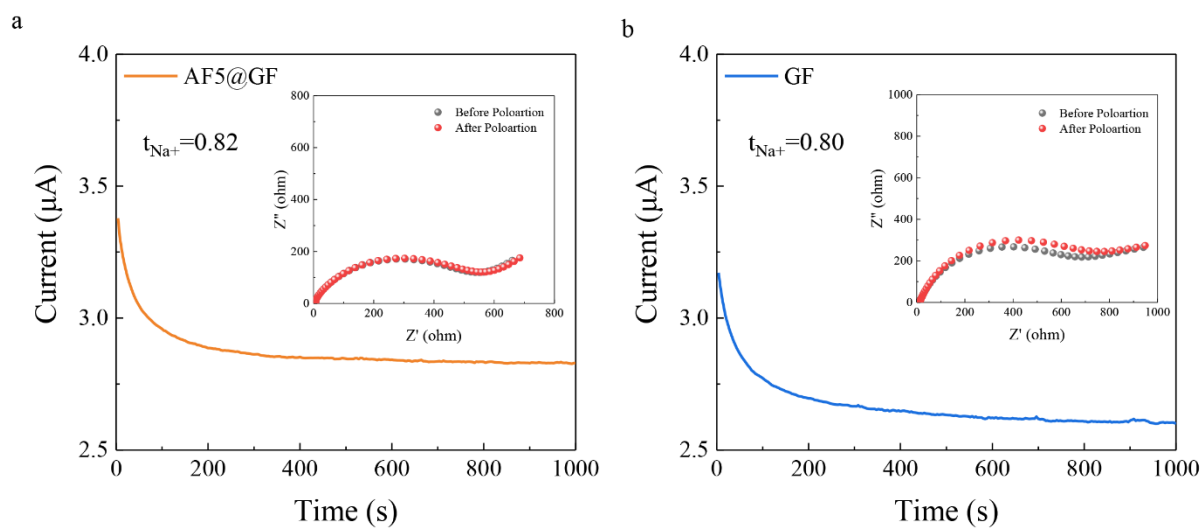


Figure S13. Polarization curve of different separators with the potential of 10 mV. Inset: Corresponding Nyquist plots before and after polarization test.

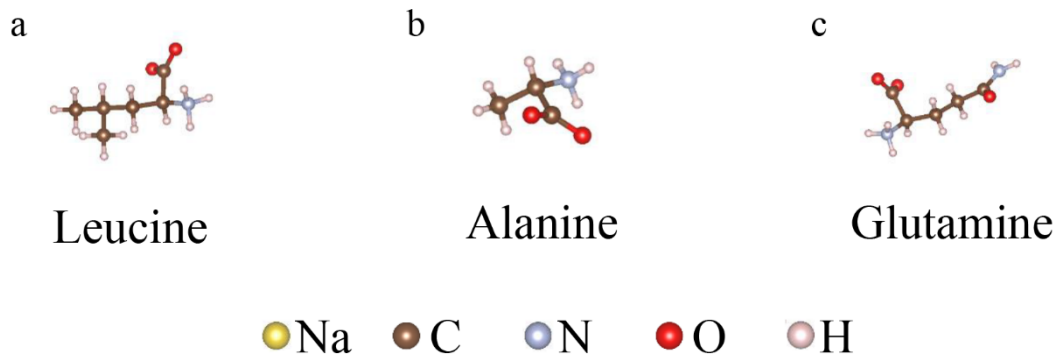


Figure S14. The three amino acid fractions in amyloid fibril. The Na, C, N, O, and H atoms are marked as yellow, brown, blue, red, and pink, respectively.

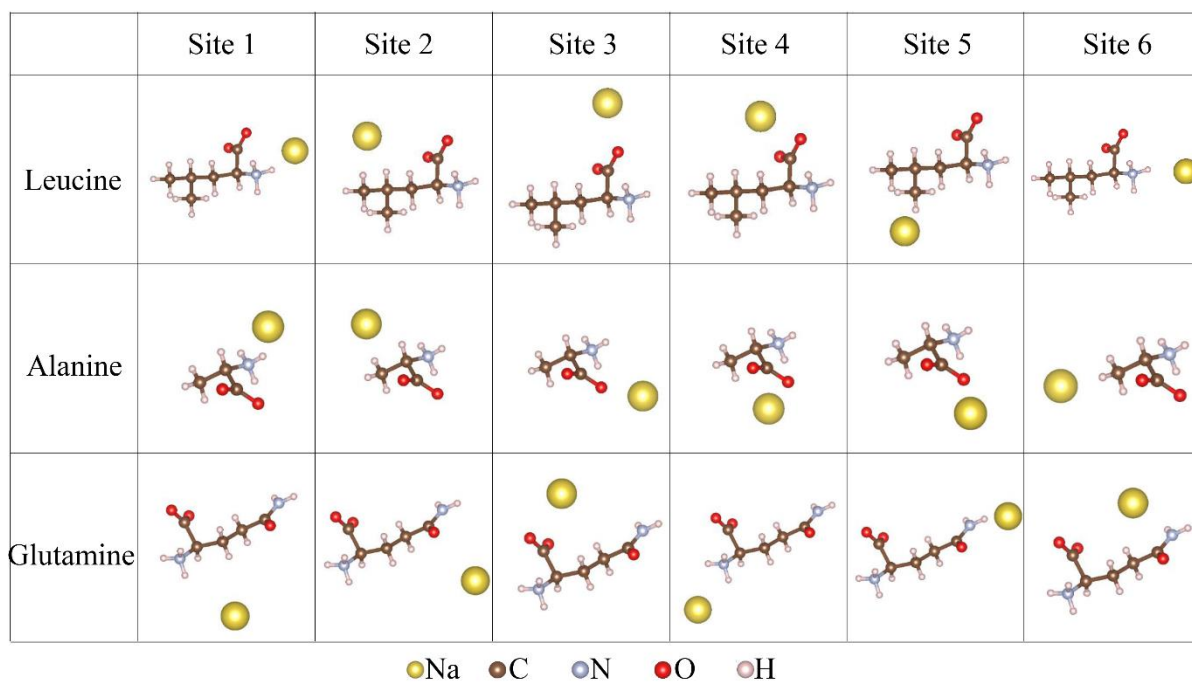


Figure S15. Initial adsorption sites states of sodium on leucine, alanine, and glutamine in amyloid fibrils.

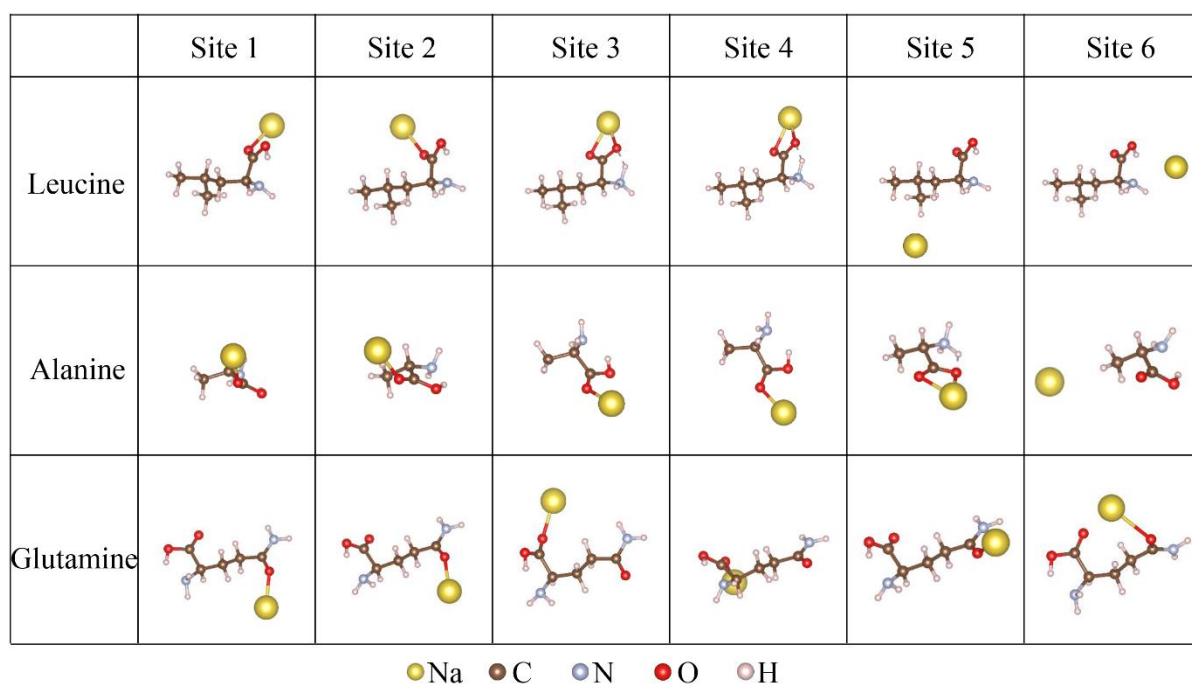


Figure S16. Stable adsorption states of sodium on leucine, alanine, and glutamine in amyloid fibrils.

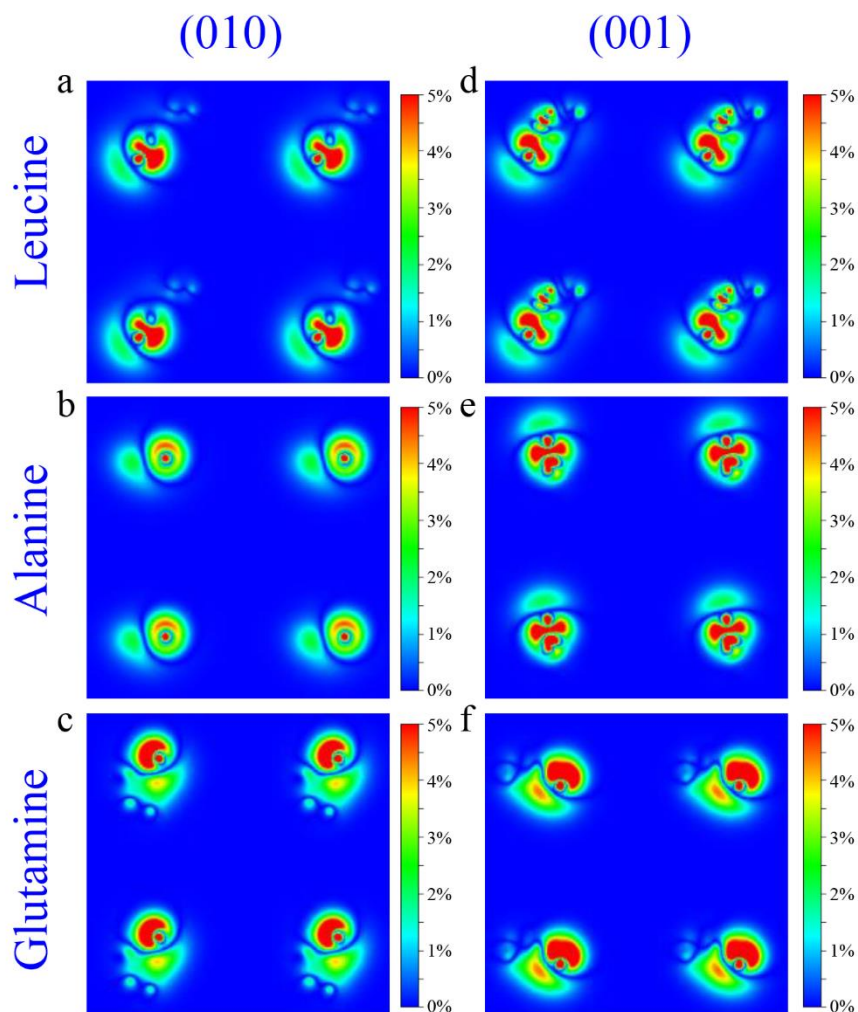


Figure S17. (a-c) The (010) plane of the charge density differences of (a) leucine, (b) alanine, and (c) glutamine with one Na atom adsorbed. (d-f) The (001) plane of the charge density differences of (d) leucine, (e) alanine, and (f) glutamine with one Na atom adsorbed.

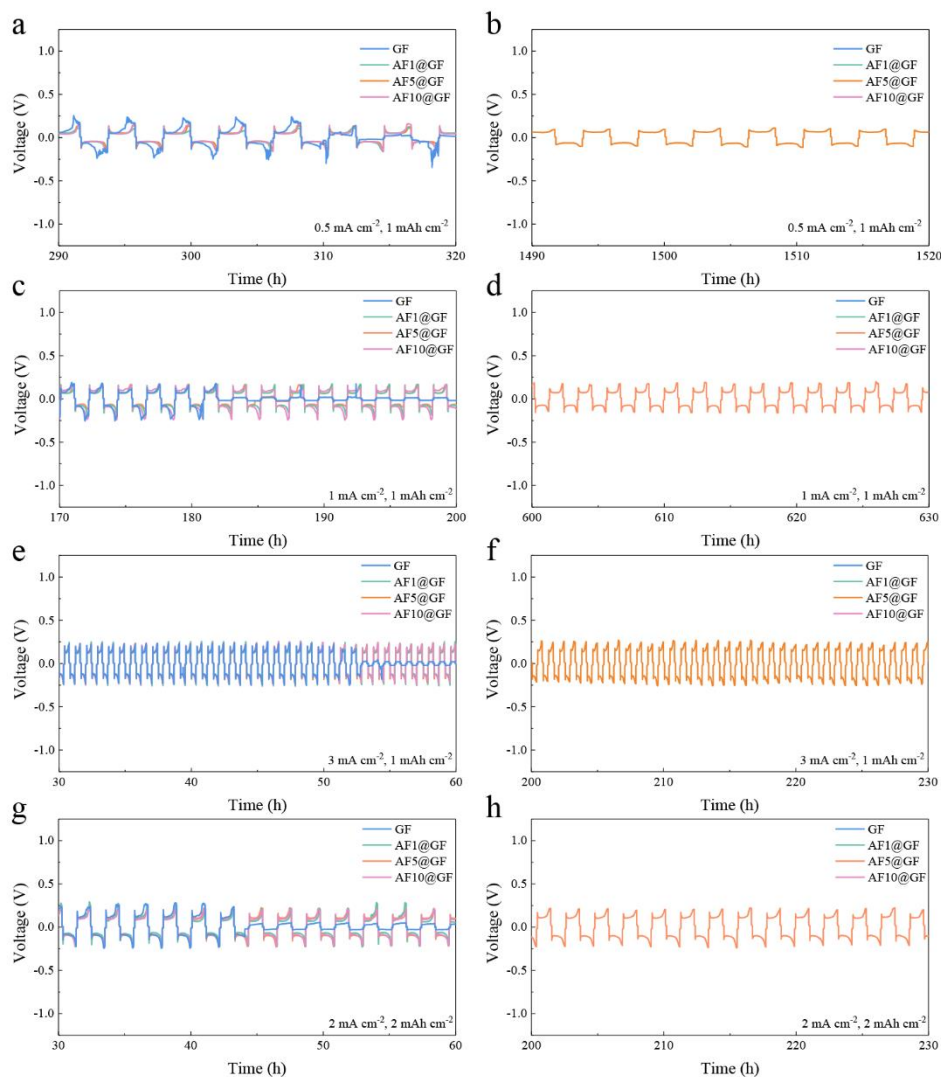


Figure S18. Details of voltage time profiles of Na plating/stripping process at 0.5 mA cm^{-2} with 1.0 mAh cm^{-2} (a-b), 1 mA cm^{-2} with 1 mAh cm^{-2} (c-d), 3 mA cm^{-2} with 1 mAh cm^{-2} (e-f), 2 mA cm^{-2} with 2 mAh cm^{-2} (g-h).

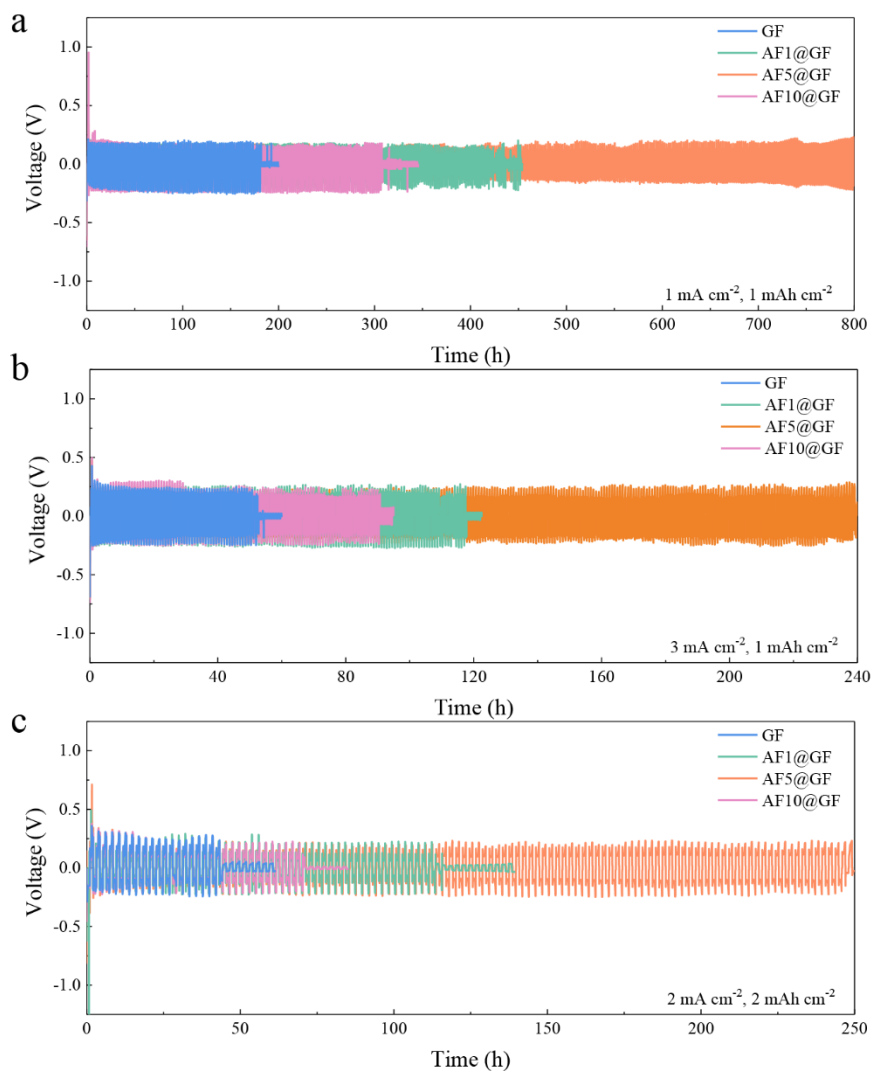


Figure S19. Voltage time profiles of Na plating/stripping process at 1 mA cm^{-2} with 1 mAh cm^{-2} (a), 3 mA cm^{-2} with 1 mAh cm^{-2} (b), 2 mA cm^{-2} with 2 mAh cm^{-2} (c).

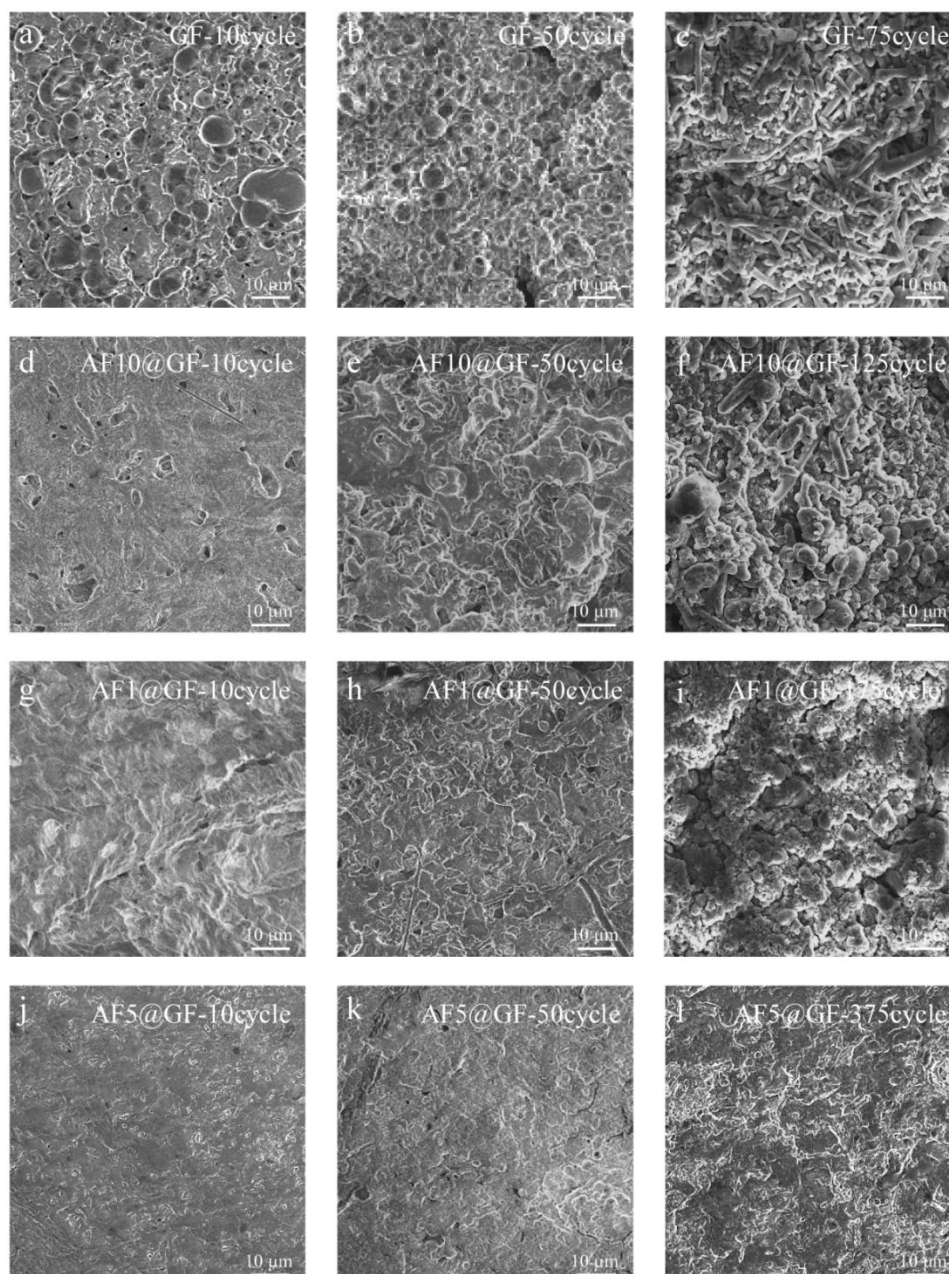


Figure S20. (a-c) SEM morphologies of Na surface after 10, 50 and 75 cycles of Na symmetric batteries with GF separator. (d-f) SEM morphologies of Na surface after 10, 50 and 125 cycles of Na symmetric batteries with AF10@GF separator. (g-i) SEM morphologies of Na surface after 10, 50 and 175 cycles of Na symmetric batteries with AF1@GF separator. (j-l) SEM morphologies of Na surface after 10, 50 and 375 cycles of Na symmetric batteries with AF5@GF separator.

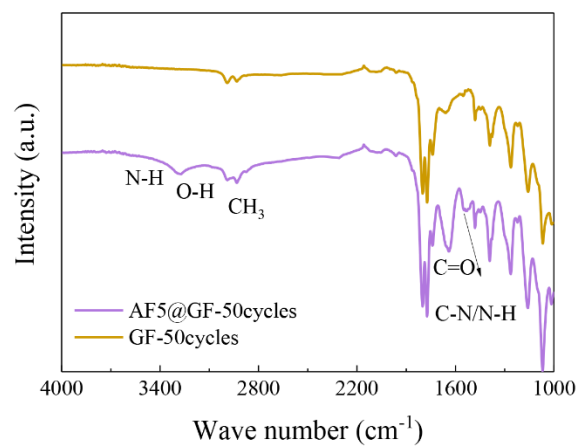


Figure S21. FTIR spectra of the AF5@GF separator and GF separator after 50 cycles.

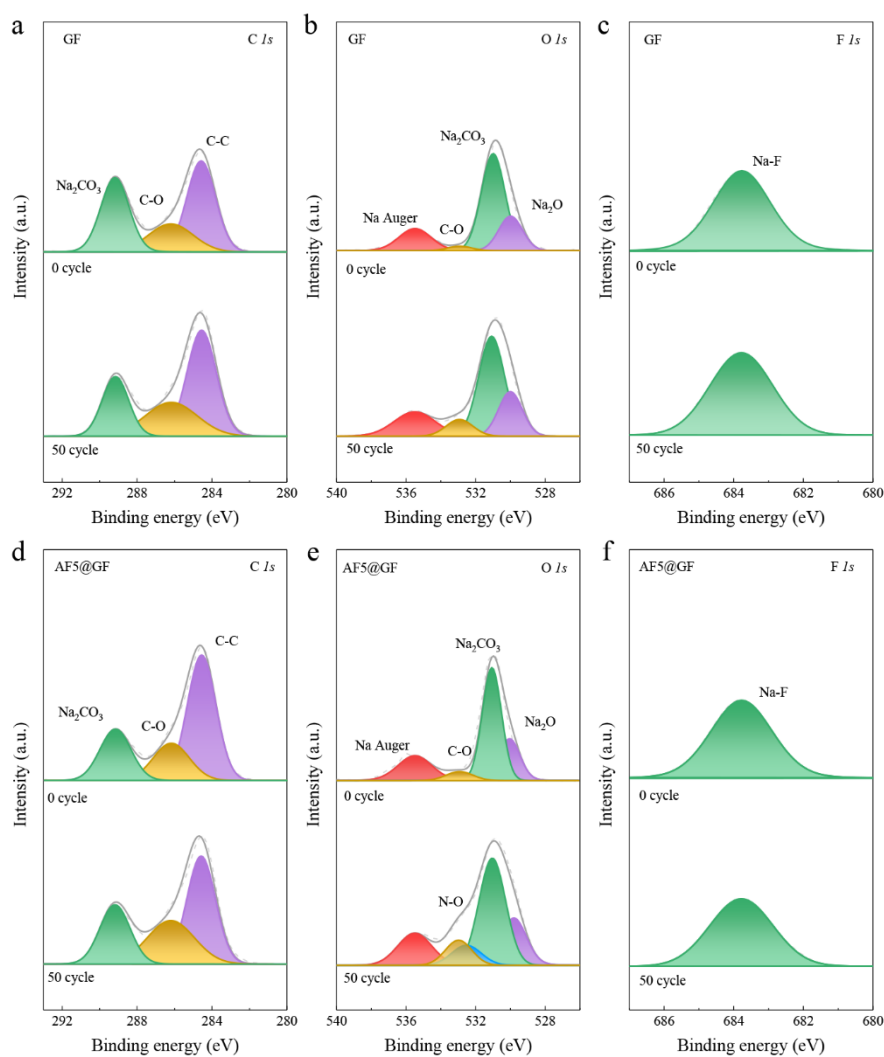


Figure S22. XPS profiles of Na anode in Na metal batteries assembled with GF (a-c) and AF@GF (d-f) separators after different cycles. (a, d) C 1s spectrum, (b, e) O 1s spectrum, and (c, f) F 1s spectrum.

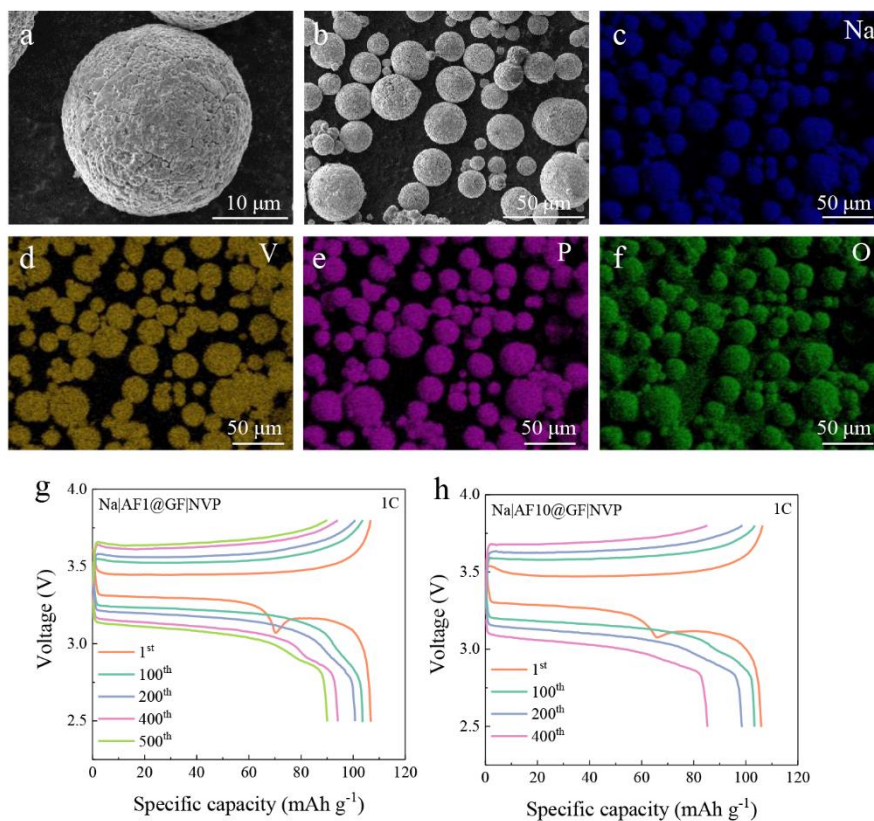


Figure S23. (a-f) SEM images of NVP cathode materials and corresponding EDS mapping. (g-h) A discharge/charge voltage profiles of the full cells of the Na|AF1@GF|NVP (g) and Na|AF10@GF|NVP (h).

Note: After the first plateau is almost completely discharged, residual sodium ions may interact with the diffusing sodium ions and impede their further diffusion, which is known as the effect of "local potential". This change in local potential causes electrons to accumulate at the electrode surface, resulting in an increase in the charge density on the electrode surface and an increase in electrode capacitance, which makes the voltage of the battery rebound slightly.

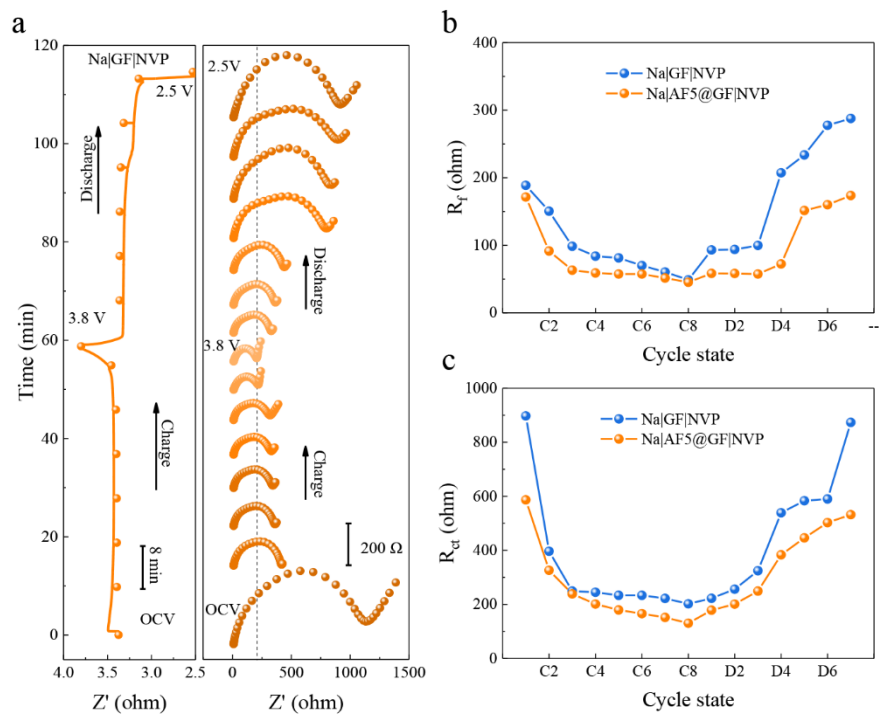


Figure S24. (a) *In-situ* EIS results of the Na|AF5@GF|NVP. (b-c) R_f values (b) and R_{ct} (c) values from the *in-situ* EIS results at different states.

Table S1. Electrochemical performance comparison of some reported materials with our work.

Materials	Electrolyte	Current density (capacity)	Cumulative capacity (cycle time)	Ref.
Al ₂ O ₃ coating	1 M NaClO ₄ in EC/DEC (1:1 = v/v)	0.5 mA cm ⁻² (1 mAh cm ⁻²)	60 mAh cm ⁻² (120 h)	[1]
Na-Sn alloy/Na ₂ O framework	1 M NaClO ₄ in EC/PC (1:1 = v/v)	0.5 mA cm ⁻² (1 mAh cm ⁻²)	162.5 mAh cm ⁻² (325 h)	[2]
Nitrofullerene	1 M NaClO ₄ in PC+EC with C ₆₀ (NO ₂) ₆	0.5 mA cm ⁻² (1 mAh cm ⁻²)	175 mAh cm ⁻² (350 h)	[3]
Al ₂ O ₃ -PVdF-HFP	1 M NaClO ₄ in EC/PC (1:1 = v/v)	0.5 mA cm ⁻² (1 mAh cm ⁻²)	254 mAh cm ⁻² (508 h)	[4]
Carbonized Mg-MOF-74	1.0 M NaClO ₄ in EC/DEC (1:1 = v/v) with 5% FEC	0.5 mA cm ⁻² (1 mAh cm ⁻²)	675 mAh cm ⁻² (1350 h)	[5]
Ultrathin graphene films	1 M NaPF ₆ in EC/DEC (1:1 = v/v)	1 mA cm ⁻² (1 mAh cm ⁻²)	200 mAh cm ⁻² (200 h)	[6]
C supported N-anchored Zn single atoms	1 M NaClO ₄ in EC/DMC (1:1 = v/v) with 5% FEC	0.5 mA cm ⁻² (0.5 mAh cm ⁻²)	500 mAh cm ⁻² (1000 h)	[7]
		1 mA cm ⁻² (1 mAh cm ⁻²)	300 mAh cm ⁻² (300 h)	
Na-wood	1 M NaClO ₄ in EC/DEC (1:1 = v/v)	0.5 mA cm ⁻² (0.25 mAh cm ⁻²)	125 mAh cm ⁻² (250 h)	[8]
		1 mA cm ⁻² (0.5 mAh cm ⁻²)	250 mAh cm ⁻² (250 h)	
		1 mA cm ⁻² (1 mAh cm ⁻²)	500 mAh cm ⁻² (500 h)	
NaBr/Na ₃ P nanocrystallines	1 M NaPF ₆ in EC/DEC (1:1 = v/v) with 5% FEC	1 mA cm ⁻² (1 mAh cm ⁻²)	700 mAh cm ⁻² (700 h)	[9]
Alucone molecular	1 M NaPF ₆ in EC/PC (1:1	3mA cm ⁻²	243 mAh cm ⁻²	[10]

layer	= v/v)	(1 mAh cm ⁻²)	(81 h)	
Na-MoS ₂	1.0 M NaClO ₄ in EC/DEC (1:1 = w/w) with 10% FEC	0.5 mA cm ⁻² (0.25 mAh cm ⁻²)	50 mAh cm ⁻² (100 h)	[11]
Na-Na ₂ S-C	1.0 M NaClO ₄ in EC/DEC (1:1 = w/w) with 10% FEC	1 mA cm ⁻² (0.5 mAh cm ⁻²)	300 mAh cm ⁻² (300 h)	[12]
3D carbon Felt	1 M NaClO ₄ in EC/PC (1:1 = v/v)	1 mA cm ⁻²	480 mAh cm ⁻²	[13]
		(2 mAh cm ⁻²)	(480 h)	
		3 mA cm ⁻² (2 mAh cm ⁻²)	480 mAh cm ⁻² (160 h)	
Na@r-GO	1m NaClO ₄ in EC/PC(1:1 = v/v)	0.5 mA cm ₂ (0.25 mAh cm ⁻²)	30 mAh cm ⁻² (60 h)	[14]
Amyloid fibril	1.0 M NaClO ₄ in EC/ DEC (1:1 = v/v) with 5wt.% FEC	0.5 mA cm ⁻²	900 mAh cm ⁻²	-
		(1 mAh cm ⁻²)	(1800 h)	
		1 mA cm ⁻²	800 mAh cm ⁻²	
		(1 mAh cm ⁻²)	(800 h)	
		2 mA cm ⁻²	500 mAh cm ⁻²	
		(2 mAh cm ⁻²)	(250 h)	
3 mA cm ⁻²	720 mAh cm ⁻²			
		(1 mAh cm ⁻²)	(240 h)	

Table S2. EIS fitting results for Na-symmetric batteries.

Samples	States	R_s (Ω)	R_{ct}+R_{SEI} (Ω)
GF	1cycle	8.852	539.6
	10cycles	9.503	331.7
	30cycles	6.586	83.43
	50cycles	8.550	509.5
AF5@GF	1cycle	7.495	207.5
	10cycles	7.247	90.44
	30cycles	10.89	58.52
	50cycles	8.144	59.71

Table S3. *In-situ* EIS fitting results for Na full cells.

State	Na AF5@GF NVP			Na GF NVP		
	Rs (Ω)	Rf (Ω)	Rct (Ω)	Rs (Ω)	Rf (Ω)	Rct (Ω)
Charge1	8.849	171.4	586.6	8.827	188.8	897.3
Charge2	8.922	91.50	326.1	8.051	150.5	396.6
Charge3	9.039	63.14	238.6	8.997	98.54	249.3
Charge4	9.923	59.03	201.2	8.940	83.92	244.8
Charge5	8.715	57.48	179.2	8.929	81.29	233.6
Charge6	8.629	57.46	165.6	8.829	69.94	233.4
Charge7	8.665	51.52	151.6	7.942	60.44	222.1
Charge8	11.71	45.30	130.2	8.448	48.78	202.0
Discharge1	11.54	58.37	178.5	8.935	93.08	222.5
Discharge2	11.66	58.32	201.1	8.949	93.83	256.3
Discharge3	11.58	57.44	249.2	8.937	99.75	324.6
Discharge4	11.46	72.34	383.5	8.875	207.2	539.0
Discharge5	11.28	151.5	446.2	8.851	233.7	583.6
Discharge6	11.27	160.1	502.6	9.075	277.6	590.1
Discharge7	11.23	173.7	532.1	8.856	287.7	873.3

References

- [1] W. Luo, C. F. Lin, O. Zhao, M. Noked, Y. Zhang, G. W. Rubloff, L. Hu, *Adv. Energy Mater.* **2017**, *7*, 1601526.
- [2] X. Zheng, W. Yang, Z. Wang, L. Huang, S. Geng, J. Wen, W. Luo, Y. Huang, *Nano Energy* **2020**, *69*, 104387.
- [3] P. Li, Z. Jiang, X. Huang, X. Lu, J. Xie, S. Cheng, *Nano Energy* **2021**, *89*, 106396.
- [4] Y.-J. Kim, H. Lee, H. Noh, J. Lee, S. Kim, M.-H. Ryou, Y. M. Lee, H.-T. Kim, *ACS Appl. Mater. Interfaces* **2017**, *9*, 6000.
- [5] M. Zhu, S. Li, B. Li, Y. Gong, Z. Du, S. Yang, *Sci. Adv.* **2019**, *5*, eaau6264.
- [6] H. Wang, C. Wang, E. Matios, W. Li, *Nano Lett.* **2017**, *17*, 6808.
- [7] T. Yang, T. Qian, Y. Sun, J. Zhong, F. Rosei, C. Yan, *Nano Lett.* **2019**, *19*, 7827.
- [8] W. Luo, Y. Zhang, S. Xu, J. Dai, E. Hitz, Y. Li, C. Yang, C. Chen, B. Liu, L. Hu, *Nano Lett.* **2017**, *17*, 3792.
- [9] Z. Luo, S. Tao, Y. Tian, L. Xu, Y. Wang, X. Cao, Y. Wang, W. Deng, G. Zou, H. Liu, *Nano Energy* **2022**, *97*, 107203.
- [10] Y. Zhao, L. V. Goncharova, Q. Zhang, P. Kaghazchi, Q. Sun, A. Lushington, B. Wang, R. Li, X. Sun, *Nano Lett.* **2017**, *17*, 5653.
- [11] D. Zhang, B. Li, S. Wang, S. Yang, *ACS Appl. Mater. Interfaces* **2017**, *9*, 40265.
- [12] W. Wu, S. Hou, C. Zhang, L. Zhang, *ACS Appl. Mater. Interfaces* **2020**, *12*, 27300.
- [13] S. S. Chi, X. G. Qi, Y. S. Hu, L. Z. Fan, *Adv. Energy Mater.* **2018**, *8*, 1702764.
- [14] A. Wang, X. Hu, H. Tang, C. Zhang, S. Liu, Y. W. Yang, Q. H. Yang, J. Luo, *Angew. Chem. Int. Ed.* **2017**, *56*, 11921.